Muscle fiber strain rates in the lower leg during ankle dorsi-/plantarflexion exercise

Hooijmans, M.T.; Veeger, T.T.J.; Mazzoli, V.; Assen, H.C. van; Groot, J.H. de; Gottwald, L.M.; ... ; Kan, H.E.

Received: 2 March 2023 | Revised: 26 September 2023 | Accepted: 27 September 2023

DOI: 10.1002/nbm.5064

RESEARCH ARTICLE

NMR IN BIOMEDICINE WILEY

Muscle fiber strain rates in the lower leg during ankle dorsi-/plantarflexion exercise

Melissa T. Hooijmans[1] | Thom T. J. Veeger[2] | Valentina Mazzoli[3] | Hans C. van Assen[4] | Jurriaan H. de Groot[5] | Lukas M. Gottwald[1] | Aart J. Nederveen[1] | Gustav J. Strijkers[6] | Hermien E. Kan[2,7]

[1]Department of Radiology and Nuclear Medicine, Amsterdam University Medical Centers, University of Amsterdam, Amsterdam Movement Sciences, Amsterdam, The Netherlands

[2]C. J. Gorter MRI Center, Department of Radiology, Leiden University Medical Center, Leiden, The Netherlands

[3]Department of Radiology, Stanford University, Stanford, California, USA

[4]Department of Radiology, Leiden University Medical Center, Leiden, The Netherlands

[5]Department of Rehabilitation Medicine, Leiden University Medical Center, Leiden, The Netherlands

[6]Department of Biomedical Engineering and Physics, Amsterdam University Medical Centers, University of Amsterdam, Amsterdam Movement Sciences, Amsterdam, The Netherlands

[7]Duchenne Center Netherlands, Leiden, The Netherlands

Correspondence
Melissa T. Hooijmans, Department of Radiology and Nuclear Medicine, Z0-174, Amsterdam University Medical Centers, Meibergdreef 9, 1105 AZ Amsterdam, The Netherlands.
Email: m.t.hooijmans@amsterdamumc.nl

Funding information
Dutch Technology Foundation TTW (DIMASK #15500). Amsterdam Movement Sciences grant, Netherlands Organization for Scientific

Abstract

Static quantitative magnetic resonance imaging (MRI) provides readouts of structural changes in diseased muscle, but current approaches lack the ability to fully explain the loss of contractile function. Muscle contractile function can be assessed using various techniques including phase-contrast MRI (PC-MRI), where strain rates are quantified. However, current two-dimensional implementations are limited in capturing the complex motion of contracting muscle in the context of its three-dimensional (3D) fiber architecture. The MR acquisitions (chemical shift-encoded water–fat separation scan, spin echo-echoplanar imaging with diffusion weighting, and two time-resolved 3D PC-MRI) wereperformed at 3 T. PC-MRI acquisitions and performed with and without load at 7.5% of the maximum voluntary dorsiflexion contraction force. Acquisitions (3 T, chemical shift-encoded water–fat separation scan, spin echo-echo planar imaging with diffusion weighting, and two time-resolved 3D PC-MRI) were performed with and without load at 7.5% of the maximum voluntary dorsiflexion contraction force. Strain rates and diffusion tensors were calculated and combined to obtain strain rates along and perpendicular to the muscle fibers in seven lower leg muscles during the dynamic dorsi-/plantarflexion movement cycle. To evaluate strain rates along the proximodistal muscle axis, muscles were divided into five equal segments. *t*-tests were used to test if cyclic strain rate patterns (amplitude > 0) were present along and perpendicular to the muscle fibers. The effects of proximal-distal location and load were evaluated using repeated measures ANOVAs. Cyclic temporal strain rate patterns along and perpendicular to the fiber were found in all muscles involved in dorsi-/plantarflexion movement ($p < 0.0017$). Strain rates along and perpendicular to the fiber were heterogeneously distributed over the length of

Abbreviations: DTI, diffusion tensor imaging; EDL, extensor digitorum longus; EPI, echo planar imaging; FOV, field of view; GCL, gastrocnemius lateralis; GCM, gastrocnemius medialis; iWLLS, iterative weighted linear least squares; MRI, magnetic resonance imaging; MVCF, maximal voluntary contraction force; PC-MRI, phase-contrast magnetic resonance imaging; PER, peroneus; SE-EPI, spin echo-echo planar imaging; SNR, signal-to-noise ratio; SOLla, soleus lateral anterior compartment; SOLma, soleus medial anterior compartment; SOLpl, soleus lateral posterior compartment; SOLpm, soleus medial posterior compartment; TA, tibialis anterior; TAdeep, tibialis anterior deep compartment; TAends, two compartments distal and proximal of the tibialis anterior without visible intramuscular tendon; Tasup, tibialis anterior superficial compartment; TP, tibialis posterior; VENC, velocity encoding.

Melissa T. Hooijmans and Thom T. J. Veeger contributed equally to this manuscript.

Research (NWO), research program VIDI, project number 917.164.90.

most muscles ($p < 0.003$). Additional loading reduced strain rates of the extensor digitorum longus and gastrocnemius lateralis muscle ($p < 0.001$). In conclusion, the lower leg muscles involved in cyclic dorsi-/plantarflexion exercise showed cyclic fiber strain rate patterns with amplitudes that varied between muscles and between the proximodistal segments within the majority of muscles.

KEYWORDS
contractile function, DTI, fiber architecture, PC-MRI, skeletal muscle

1 | INTRODUCTION

Quantitative magnetic resonance imaging (MRI) is increasingly used to quantify healthy muscle architecture and architectural changes due to, for example, muscle disease, aging, injury, and training interventions.[1] Muscle architectural features, including the pennation angle, fiber length, and muscle volume, are important determinants of muscle function,[2–4] but also common compositional changes in disease, such as fibrosis and myosteatosis, influence muscle function.[5,6] Muscle composition and architecture can be assessed using a combination of quantitative MRI techniques, including chemical shift-based water–fat separation methods like the Dixon technique, T2 or T1 relaxometry, and diffusion tensor imaging (DTI).[1] However, static (qualitative and quantitative) MR readouts frequently fail to fully explain the loss of muscle function, particularly in neuromuscular diseases. For example, the gradual decrease in muscle strength characterizing various muscle diseases and sarcopenia cannot be solely explained by the loss in muscle volume.[5–7] This suggests that in these diseases there is a change in contractile function of the remaining muscle tissue that goes undetected using static MRI methods.

Muscle strain can provide a window on muscle contractile function, where strain is a local property of tissue that indicates the relative shortening or lengthening of tissue in a given direction. In skeletal muscle, strain rate (change in strain with respect to time) and strain have been examined using two-dimensional (2D) ultrasound and various MRI techniques.[8-16] 2D ultrasound generates high spatial and temporal resolution images,[17,18] but lacks the coverage and depth needed to assess full muscle strain distributions.[19] MRI has the ability to capture complete muscle volumes of multiple muscles simultaneously, but to date has been primarily focused on specific muscle parts or planes[8,11,20] using 2D implementations to reduce the scan time. However, from studies in healthy muscle tissue, it is known that both architectural characteristics (e.g., pennation angle) and more functional features (e.g.,microvascular function), vary between and within individual muscles,[8,9,13,21-29] making such 2D implementations and focused studies incomplete. At the same time, this also indicates that it is generally impossible to define a MRI plane aligned with the muscle fibers, particularly during exercise when fibers are moving and deforming.[8,30] From strain measurements themselves it is not possible to infer the underlying fiber architecture, but combined with DTI, strain can be calculated along and perpendicular to the muscle fibers. Additionally, the introduction of accelerated MRI facilitates multi-slice[22] and whole muscle assessment[30] of the three-dimensional (3D) strain rate tensor with high temporal resolution (10 ms).[30] The combination of these techniques may create 3D strain distributions of full muscle volumes in relation with principal fiber directions to explore contractile function in skeletal muscle. This could be of specific interest for various muscle diseases and in sarcopenia where the lack of muscle function cannot be fully explained by the loss in muscle volume. Hence, an advanced understanding of the role that contractile function may have in the decline in function in this population is essential, with the prospect of developing strategies aiming to preserve and/or improve muscle function.

Therefore, the main aim of this study was to assess whether 3D strain rate patterns can be measured along principal muscle fiber directions in the full volume of seven lower leg muscles during a cyclic dorsi-/plantarflexion exercise, using an in-house–developed accelerated time-resolved 3D PC-MRI protocol in combination with DT-MRI. As a first application of this technology we investigated the (in)-homogeneity of muscle fiber strain rates along the proximodistal muscle axis of the leg muscles. Moreover, to assess strain rate in a condition more similar to a daily life situation, we assessed whether the muscle fiber strain rates changed with an additional load. Based on the incompressibility phenomenon during muscle contraction,[31] we hypothesize that muscles/muscle fibers of the lower leg involved in the dorsi-/plantarflexion movement will shorten along the fiber during the contraction phase of the movement and concomitantly will expand perpendicular to the fiber. During the relaxation phase of the movement the opposite behavior is expected, thereby introducing cyclic behavior. Based on the previously reported heterogeneously distributed architectural and functional features in skeletal muscle, we hypothesize that strain rate amplitudes along and perpendicular to the fiber are also heterogeneously distributed along the proximodistal muscle axis. Lastly, with increasing load, a different execution of the dorsi-/plantarflexion movement is required and therefore differing strain rate amplitudes are expected in both the dorsiflexor and plantarflexor muscles compared with the unloaded condition.

2 | MATERIALS AND METHODS

2.1 | Participants

We collected data in the right lower leg of 12 healthy participants (age: 31.6 ± 15.9 years; six males and six females; body mass index: 23.2 ± 3.4 kg/m^2; weight: 78 ± 14.6 kg, dominant leg right/left: 10/2). The inclusion criteria were no MRI contraindication, age 18 years or older, and no injuries or complaints of the lower extremity muscles. The study was approved by the institutional medical ethical committee according to the Medical Research Involving Human Subjects Act (WMO) and all participants provided written informed consent before participation.

2.2 | Maximal voluntary contraction force measurements

First, the maximal voluntary isometric contraction force (MVCF) was assessed for the dorsi-flexor muscles using a handheld dynamometer (MicroFET2; Hoggan Scientific, Salt Lake City, UT, USA). The participants were positioned in the supine position with an extended knee and the ankle in neutral position (0°). The dynamometer was placed on the forefoot, just distal to the toes, for each of the participants. The participants performed a maximal contraction against the dynamometer and repeated this three times. If the force kept increasing or if the difference between the measurements was more than 10%, up to two extra contractions were performed. The largest force recorded during these trials was considered to be the MVCF.

2.3 | MR data acquisition

MR datasets were acquired in the right lower leg on a 3-T MR System (Philips, Ingenia, Best, The Netherlands) using a 16-element receiver coil (anterior) and the 10-element receiver coil built into the patient table (posterior). The participants were positioned supine feet-first in the MR scanner with the right leg as close as possible to the center of the bore. The anterior coil was placed on top of the legs and supported with foam pillows and fixation bands to ensure that the coil covered the full lower leg and did not move during ankle dorsi-/plantarflexion movement. The MR examination consisted of two parts with a total duration of 65 min, including repositioning in between the scans. The first part of the MR examination was performed with the ankle passively held in neutral angle (0°) to determine muscle fiber orientations and consisted of the following scans:

I. I. Chemical shift-based water–fat separation scan (3D fast field echo [FFE]; mDIXON quant [multiecho]; TR/TE/ΔTE/FA 7.8/1.27/1.1 ms/3°; six echoes; recon voxel size 1 × 1 × 3 mm^3; number of signal averages: 1; acquisition matrix: 192 × 192; number of slices: 130; scan duration: 70.1 s) for muscle segmentation.
II. Diffusion-weighted acquisition to assess principal fiber directions (spin echo-echo planar imaging [SE-EPI]; TR/TE: 6123/48 ms; 24 directions; b-values: 0 (5), 400 (19) s/mm^2; recon voxel size: 3 × 3 × 6 mm^3; number of signal averages: 1; acquisition matrix: 64 × 64; number of slices: 65; no slice gap, SENSE 1.9; combination of three fat suppression techniques: SPectral Adiabatic Inversion Recovery (SPAIR) and Slice Selected Gradient Reversal (SSGR) for the main aliphatic fat peak and a SPIR pulse for the olefinic fat peak; partial Fourier factor: 0.73; scan duration: 290 s).

After changing the setup to facilitate the exercise task, the second part of the MR examination focused on retrieving velocity information during dynamic unconstrained dorsi-/plantarflexion movement with and without load, using the following scans:

I. Chemical shift-based water–fat separation scan (3D FFE; mDIXON quant [multiecho]; TR/TE/ΔTE/FA 7.8/1.27/1.1 ms/3°; six echoes; recon voxel size 1 × 1 × 3 mm^3; number of signal averages: 1; acquisition matrix: 192 × 192; number of slices: 130; scan duration: 70.1 s) for muscle segmentation in the neutral foot position.
II. Two time-resolved 3D PC-MRI acquisitions to retrieve velocity information during dorsi-/plantarflexion movement at 0.5 Hz (starting in plantarflexion), one with and one without load (FFE; TR/TE = 9.4/4.4 ms; velocity encoding [VENC] = 10 cm/s; three velocity-encoding directions; 20 time-steps, recon voxel size: 3 × 3 × 6 mm^3; no fat suppression; scan duration of 432 s corresponding to 216 motion task repetitions) covering the full lower leg (field of view [FOV]: 192 × 192 × 390 mm^3). The 216 motion task repetitions were needed to acquire the images of the 20 time-steps for the full FOV, resulting in one set of images representing one single movement cycle. The additionally applied load was 7.5% of the MVCF and conservatively chosen according to previous used (10%–40% MVCF) literature values in combination with the length of our MR acquisition, which was substantially longer compared with previous work.[28,32,33] Time-resolved 3D PC-MRI data were acquired by incoherently undersampling k-space based on a pseudo-spiral pattern (undersampling factor: R = 9.1 with respect to a fully sampled dataset).[34]

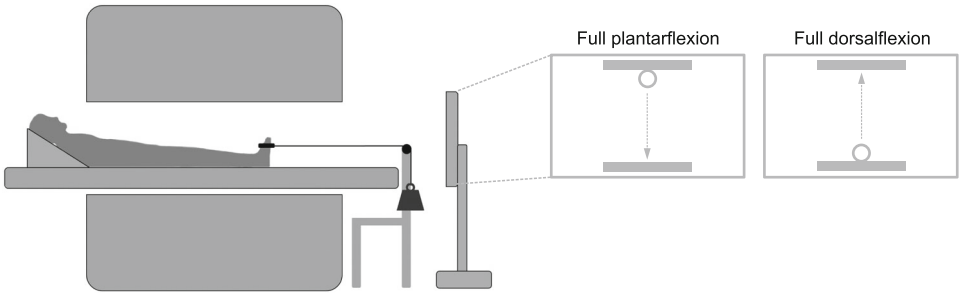

FIGURE 1 A schematic overview of the exercise setup. The participants were positioned supine and were shown a screen for visual feedback of the motion task. The participants were asked to perform a dynamic dorsi-/plantarflexion movement every 2 s, starting in the plantar flexed position. For the load condition, a weight (7.5% of maximum voluntary contraction force) was attached to the ankle by a strap on the dorsal side of the foot.

The proximal end of the slice stack was positioned at the level of the tibia plateau and the midline of the imaging stack was aligned with the tibia bone for each of the MR sequences. A schematic representation of the exercise setup is shown in Figure 1. The television screen displayed a moving tennis ball, which was used to synchronize the dynamic dorsi-/plantarflexion movement cycle with the acquisition. For each participant the unloaded condition was acquired first. After a short break of 5 min the data were acquired during the condition with load.

2.4 | Postprocessing

A schematic workflow of the postprocessing and data analysis steps is shown in Figure 2. All data were visually assessed for movement and fat artifacts by one observer with more than 10 years' experience in MSK MRI, specifically in skeletal muscle. Chemical shift-based water–fat separation Dixon scans were reconstructed using scanner software. Diffusion datasets were processed using QMRITools (https://github.com/mfroeling/QMRITools) for Wolfram Mathematica 12. The diffusion data were de-noised using a principal component analysis algorithm and the diffusion-weighted images were spatially registered to b = 0 images to correct for motion- and eddy current-induced displacements using elastix (https://elastix.lumc.nl/; 26 August 2022).[35] Thereafter, the diffusion data were registered to the Dixon water images acquired just prior to the DTI acquisition, using a rigid registration and a B-spline registration to correct for EPI distortions. The diffusion tensor was calculated per voxel using an iterative weighted linear least squares (iWLLS) algorithm. The tensor was diagonalized, generating three eigenvectors (ev_1, ev_2, ev_3) per voxel. Signal-to-noise ratios (SNRs) were calculated per voxel based on the local average signal divided by the local noise sigma. DTI signal was determined on the b = 0 image, while the noise sigma was based on the background signal.[36] Datasets with SNRs of less than 20 were excluded from the analysis.

PC-MRI data were reconstructed using a Compressed Sensing pipeline[34] using BART. As a first step, the average velocity over all voxels and over the complete movement cycle was calculated and subtracted from the velocity data in order to exclude signal drift artifacts in the cyclic movement.[9,30] The resulting velocity data were then de-noised using a first order Gaussian filter (sigma = 1 voxel; through plane sigma = 0.5 voxels) and used to calculate the 3D spatial gradient, the Jacobian (*J*) per voxel per frame (time):

$$J = \begin{bmatrix} \frac{\partial v_x}{\partial x} & \frac{\partial v_x}{\partial y} & \frac{\partial v_x}{\partial z} \\ \frac{\partial v_y}{\partial x} & \frac{\partial v_y}{\partial y} & \frac{\partial v_z}{\partial z} \\ \frac{\partial v_x}{\partial x} & \frac{\partial v_y}{\partial y} & \frac{\partial v_z}{\partial z} \end{bmatrix}. \quad (1)$$

From *J* the infinitesimal strain rate tensor (*S*) per voxel per frame (time) was calculated:

$$S(t) = \frac{1}{2}\left(J(t) + J(t)^T\right). \quad (2)$$

This resulted in 3D strain rate tensor maps and 3D muscle fiber eigenvector maps for the full lower leg with a spatial resolution of $3 \times 3 \times 6$ mm^3 and a temporal resolution of 100 ms. These 3D maps were used as the input for further data analysis.

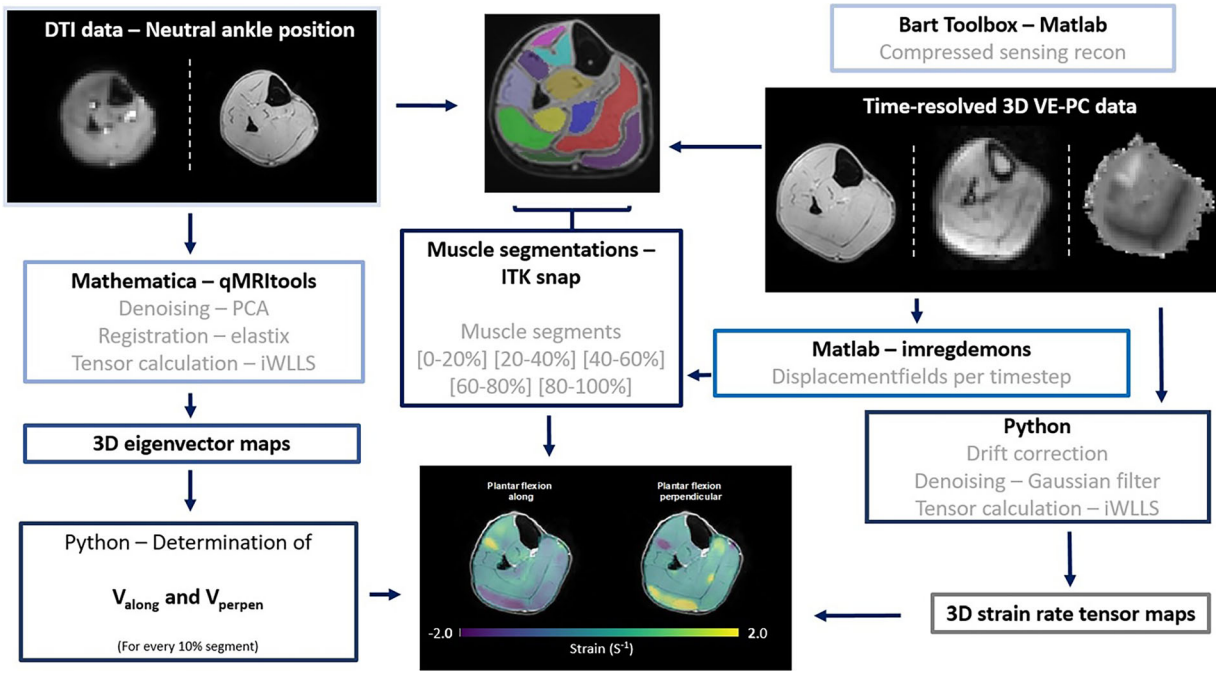

FIGURE 2 A flowchart describing the analysis steps and the analysis tools and programs used to derive the strain rates along and perpendicular to the fibers. 3D, three-dimensional; DTI, diffusion tensor imaging; iWLLS, iterative weighted linear least squares; PCA, principal component analysis.

2.5 | Data analysis

Volumes of interest (VOIs) were manually drawn using the scanner-reconstructed water images of the two Dixon acquisitions in the neutral foot position. The VOIs were drawn inside the border of the muscles along the full length of seven lower leg muscles for the fiber orientation (on the first acquired Dixon acquisition) and the velocity (on the second acquired Dixon acquisition) datasets separately using ITK-snap (www.itksnap.org; version 3.6.0; April 2017).[37] Seven lower leg muscles were analyzed, that is, the tibialis anterior (TA), tibialis posterior (TP), extensor digitorum longus (EDL), peroneus (PER), soleus (SOL), gastrocnemius medialis (GCM), and gastrocnemius lateralis (GCL) muscles (Figure 3). Additionally, the SOL and TA were subdivided into smaller VOIs to account for the different compartments of these muscles.[8,38] For the SOL muscle, a lateral anterior compartment (SOLla), a medial anterior compartment (SOLma), a lateral posterior compartment (SOLlp), and a medial posterior compartment (SOLmp) were defined (Figure 3). The TA was subdivided into two compartments in the middle section where the muscle is separated by the intramuscular tendon, namely, the superficial (TAsup) and the deep (TAdeep) compartments. Distal and proximal to the muscle belly, without a visible intramuscular tendon, the TA was drawn as one compartment (TAends) (Figure 3). The VOIs for the full TA muscle and SOL muscle were generated by combining the VOIs for the individual compartments. The reconstructed water images used for VOI selection were subsequently registered to individual time-steps[20] of the PC-MRI data (magnitude images) using the built-in *imregdemons* function in Matlab (version: 2019a), and the deformation matrices resulting from the registration were used to deform the VOIs to all the individual PC time-steps. Finally, the full muscle volumes were divided into five equal segments based on the normalized muscle length (i.e., distal segment [0%–20%]; segment 20%–40%; segment 40%–60%; segment 60%–80%; and proximal segment [80%–100%]). Four muscle compartments were only represented in the three midsegments, covering 20%–80% of the muscle (Figure 3).

To calculate strain rates along and perpendicular to the fiber, our DTI and PC-MRI datasets had to be combined. Unfortunately, a voxel-by-voxel comparison was difficult because of differences in resolution and acquisition setup. Therefore, first, the most prominent fiber direction for every VOI was calculated as the weighted average principal eigenvector (ev_1) from the DTI (V_{along}) for every 10% section (s10%) of the total muscle length (Equation 3). Because of the circular cross-sectional shape of the fiber, the two perpendicular eigenvectors (ev_2 and ev_3) were interchangeable and dependent on the surroundings, and an average was not useful. Instead, the average principal fiber direction was used to define the cross-sectional plane of the fiber, by calculating vectors pointing in the two perpendicular directions in the plane perpendicular to V_{along} (V_{p1} and V_{p2}; Equations 4.1 and 4.2, respectively):

$$V_{along,s10\%} = \frac{\overline{ev_1}}{\|ev_1\|} \tag{3}$$

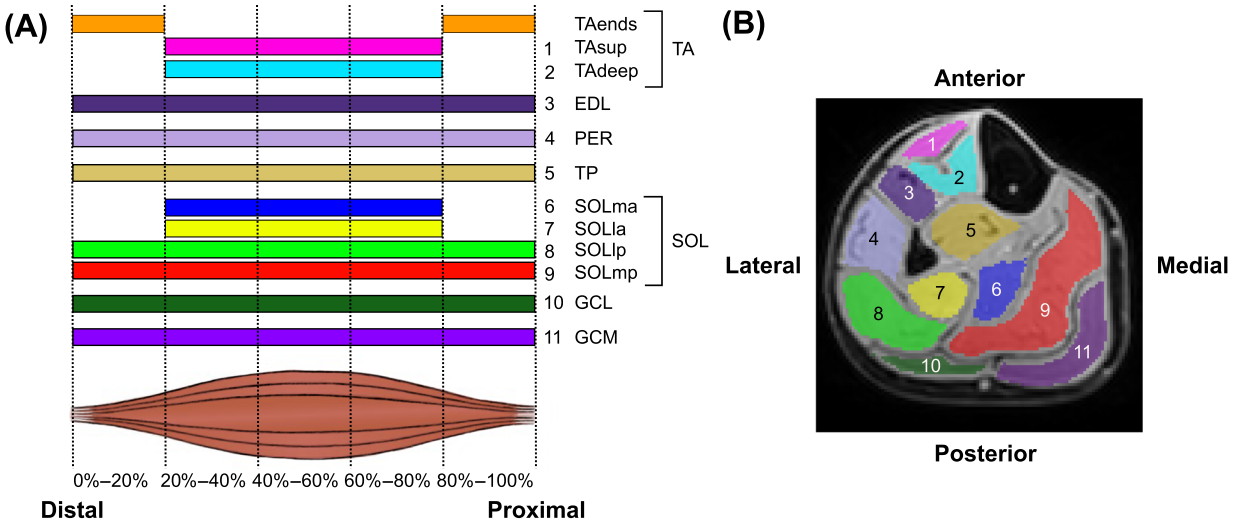

FIGURE 3 An overview of the manually segmented muscles and muscle compartments. Regions of interest for the individual muscles and muscle compartments (B) and their distribution along the length of the lower leg (A). TAends, two compartments distal and proximal of the tibialis anterior without visible intramuscular tendon; (1) TAsup, superficial compartment of the tibialis anterior; (2) TAdeep, deep compartment of the tibialis anterior; (3) EDL, extensor digitorum longus; (4) PER, peroneus; (5) TP, tibialis posterior; (6) SOLma, medial anterior compartment of the soleus muscle; (7) SOLla, lateral anterior compartment of the soleus muscle; (8) SOLlp, lateral posterior compartment of the soleus muscle; (9) SOLmp, medial posterior compartment of the soleus muscle; (10) GCL, lateral head of the gastrocnemius muscle; (11) GCM, medial head of the gastrocnemius muscle. SOL, soleus; TA, tibialis posterior.

$$V_{p1} = \frac{V_{along} \times [0\ 1\ 0]}{\left\| V_{along} \times [0\ \ 1\ \ 0] \right\|} \tag{4.1}$$

$$V_{p2} = \frac{V_{along} \times V_{p1}}{\left\| V_{along} \times V_{p1} \right\|} \tag{4.2}$$

These three unit vectors (V_{along}, V_{p1}, V_{p2}) were then used to calculate the strain rate in these directions (SR_{along}, SR_{p1}, SR_{p2}) on a voxel-by-voxel basis within all VOIs:

$$SR(t) = V_{s10\%}{}^{T} \cdot S(t) \cdot V_{s10\%} \tag{5}$$

with t indicating every time point.

To obtain one strain rate measure resembling the expansion and compression in the perpendicular cross-sectional plane, with the same order of magnitude as the strain rate along the fiber, the perpendicular cross-sectional area (CSA) strain rate ($\overline{SR_{pCSA}}$) was calculated. First, SR_{p1} and SR_{p2} were used to calculate $\overline{SR_p}$, the average strain rate over the two directions (Equation 5.1). $\overline{SR_p}$ was then used to calculate ($\overline{SR_{pCSA}}$), on a voxel-by-voxel basis using Equations (5.2) and (5.3):

$$\overline{SR_p}(t) = \frac{SR_{p1}(t) + SR_{p2}(t)}{2} \tag{5.1}$$

$$\overline{SR_{CSAp}}(t) > 0 : \overline{SR_p}(t) = \pi \cdot \overline{SR_p}(t)^2 \tag{5.2}$$

$$\overline{SR_{CSAp}}(t) < 0 : \overline{SR_p}(t) = -\pi \cdot \overline{SR_p}(t)^2 \tag{5.3}$$

The negative π was used to maintain the sign of strain rate. Weighted average and standard deviations were calculated for SR_{along} and SR_{perpen} for all five segmented VOIs from distal to proximal (0%:20%; 20%:40%; 40%:60%; 60%:80%, 80%–100%) over time. This resulted in two strain rates, that is, along the fiber direction (SR_{along}), and in the plane perpendicular to the fiber direction (SR_{perpen}). Using these five segments for the weighted analysis ensured a sufficient number of pixels per VOI region. The average number of pixels over all participants of the two outer segments, most probably affected by the low number of pixels, for each of the muscle/muscle compartments, ranged from 68–301 pixels (0%–20% segment) to 165–1012 pixels (80%–100% segment).

Visual inspection of the data displayed smooth cyclic wavelike patterns, in line with previous work.[9,30] Therefore, we first modeled the resulting velocity time series to follow a simple sinusoidal pattern with a frequency of 0.5 Hz (i.e., one full cycle over 2 s). This cyclic wavelike trajectory is either starting with negative strain rates, or counterclockwise, starting with positive strain rates. Therefore, to enable comparisons between time series, a sinusoidal function with a frequency of 0.5 Hz was fitted to the data using a least squares method:

$$SR(t) = A \cdot sin(\pi t) + B \tag{6}$$

with A the amplitude constrained between -5 and 5. Negative A indicates shortening/thinning and positive A indicates lengthening/thickening, and B the offset from zero. The suitability and quality of the sinusoidal fit was evaluated according to visual inspection by MH and TV. In case of unsuitability of the sinusoidal fit, more complex models were explored.

2.6 | Statistical analysis

Statistical analyses were performed using R (R Core Team, 2019) using the package *lme4* (Bates 2015). All datasets were checked for normality and statistical tests were selected accordingly. To assess the wavelike behavior for every muscle along and perpendicular to the fiber, one-sided *t*-tests, assuming equal variance, or Wilcoxon signed-rank tests, were used to test if the average strain rate amplitudes (two amplitudes for every muscle/muscle compartment, along and perpendicular to the fiber) over all participants were different from zero. The effect of load and proximal-distal location on strain rates along and perpendicular to the fiber for all muscles and compartments was assessed using multiple repeated measures ANOVAs, using a linear mixed model approach. These models included the strain rate amplitude (A) from the sinusoidal fits as outcome variable. The factors' load condition (two levels; load or no load) and proximodistal segment (five levels) were added as independent predictors for strain rate amplitude A, including their interaction. Last, a by-participant random intercept was added to each model. For all tests the level of statistical significance was corrected for multiple testing (Bonferroni) and was set at p less than or equal to 0.0018 (i.e., 0.05/28 statistical tests, 14 muscle [−compartments] × 2 directions).

3 | RESULTS

3.1 | Study population and data quality

The dorsiflexion MVCF measured at the foot of our participants was 262.2 ± 57.7 N and ranged from 185.5 to 411.5 N, which is in line within the normal range.[39] None of the MRI datasets showed any motion or fat artifacts and all diffusion datasets were of sufficient SNR (> 20) and thus were included in the statistical analyses.

3.2 | Temporal pattern of strain rates

Representative images color-coded for strain rate along and perpendicular to the fibers for one subject during maximal dorsiflexion velocity and maximal plantarflexion velocity without load are shown in Figure 4. Based on careful visual inspection, it was evident that the sinuisodal fit provided a suitable description of the data. In most lower leg muscles a cyclic temporal pattern, meaning an amplitude different from zero, was found for strain rates along and perpendicular to the fiber ($p < 0.0018$), with varying amplitudes between muscles (Table 1).

For the GCM and GCL muscle, positive strain rates along the fiber related to ankle dorsiflexion, indicating lengthening of fibers, and negative strain rates perpendicular to the fibers, indicating thinning of fibers, were seen (Figure 5). During ankle plantarflexion, the opposite was observed, with negative strain rates along (i.e., shortening) and positive strain rates perpendicular to (i.e., thickening) the muscle fiber (Figure 5). For the SOL muscle as a whole a cyclic pattern was observed, but with smaller strain rate amplitudes along and perpendicular to the fibers in comparison with the GCM and GCL muscles during both the dorsi- and plantarflexion phase (Table 1 and red dashed lines in Figure 5). The individual compartments of the SOL muscle, however, showed more variability in strain rate amplitudes than the other plantar flexor muscles (Table 1 and red dashed lines in Figure 6). In the SOLla and SOLmp compartments, cyclic patterns were measured along and perpendicular to the fiber, in the SOLma compartment only along the fiber, whereas in the SOLlp compartment a cyclic pattern in strain rate amplitudes, along and perpendicular to the muscle fibers, was absent ($p > 0.0018$).

In the antagonist TA and EDL muscles, an opposed cyclic pattern, compared with the plantarflexion muscles, was observed. This consisted of negative strain rate amplitudes along the fibers and positive strain rate amplitudes perpendicular to the fibers during ankle dorsiflexion, while this was the opposite during plantarflexion (Table 1 and the red dashed lines in Figures 7 and 8). The compartment analysis of the TA muscle was

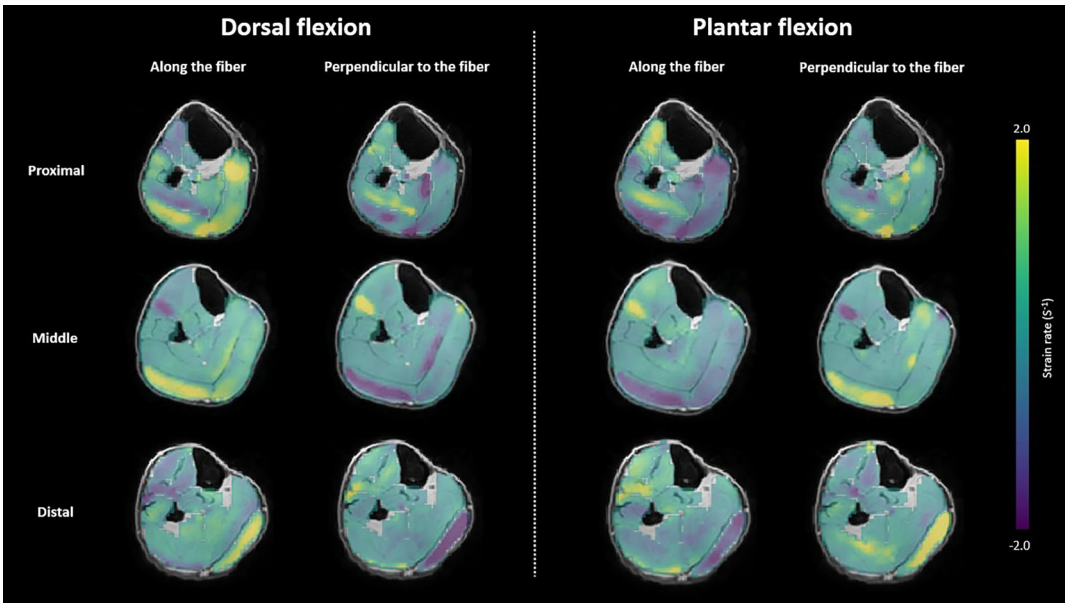

FIGURE 4 Example of cross-sectional images (segment 20%–40% [distal]; segment 40%–60% [middle]; and segment 60%–80% [proximal]) of the lower leg with color-coded strain rate amplitude along (left) and perpendicular (right) to the fiber during maximal dorsiflexion (left) and maximal plantarflexion (right) phase of the movement. Note the general antagonistic behavior in the anterior and posterior compartment of the lower leg and the difference between the individual slices.

similar to the one for the full muscle. In the TP and PER muscles, cyclic patterns in strain rate amplitudes were absent both along and perpendicular to the muscle fibers ($p > 0.0018$) (Table 1 and Figure 8).

3.3 | Proximodistal distribution of strain rates

The majority of the analyzed lower leg muscles showed an effect of proximodistal location on the strain rate amplitudes along the fibers (Table 2), except for the SOL muscle and SOL compartments. Strain rates perpendicular to the fibers were also heterogeneously distributed over the length of the muscle in the majority of muscles and muscle compartments, except for the TP muscle and the TAends compartment (Table 2). The distribution of strain rate amplitudes along and perpendicular to the fibers was not consistent over all muscles. In general, the absolute strain rate tended to increase either towards the proximal or distal muscle insertion. This resulted in the highest absolute strain rates in the 0%–20% and 80%–100% segments (i.e., TA; Figure 7), or in the 20%–40% and 60%–80% segments (i.e., GCL; Figure 5). In the TAsup compartment, even opposite behavior between the most distal segment compared with the two other segments was seen, with negative amplitudes in the distal segment (20%–40%) and positive amplitudes in the rest of the muscle segments (40%–60% and 60%–80%) (Figure 7). There are some small variations in this pattern between individual participants; this is shown for the EDL muscle in Figure S1.

3.4 | Load effect

An effect of load on strain rate amplitudes along and perpendicular to the fiber was observed in the EDL and GCL (Table 2 and Figures S2–S5). In both muscles, lower strain rate amplitudes were measured in the loaded condition compared with the condition without load ($p < 0.0001$; $p < 0.0001$). None of the other muscles displayed an effect of load on strain rate amplitudes along and perpendicular to the fiber ($p > 0.0001$).

4 | DISCUSSION

This study demonstrates that it is feasible to assess strain rate along and perpendicular to muscle fibers covering the entire lower leg during dynamic dorsi-/plantarflexion exercise, using a combination of PC-MRI and DTI. The lower leg muscles and muscle compartments involved in repetitive dorsi-/plantarflexion movements exhibited cyclic temporal patterns for strain rates along and perpendicular to the fibers for the full 3D

TABLE 1 *t*-test results.

		Along the fiber					Perpendicular to the fiber				
Muscles	Compartments	Mean amplitude	SD	CI	*t*	*p* value	Mean amplitude	SD	CI	t	*p* value
GCL		0.53	0.22	0.39 to 0.67	8.3	< 0.0001	−0.44	0.21	−0.57 to −0.30	−7.18	< 0.0001
GCM		0.47	0.12	0.40 to 0.55	13.73	< 0.0001	−0.14	0.08	−0.19 to −0.10	−6.57	< 0.0001
SOL		0.17	0.08	0.12 to 0.22	7.49	< 0.0001	−0.11	0.05	−0.14 to −0.08	7.08	< 0.0001
	SOLla	0.25	0.13	0.17 to 0.33	6.75	< 0.0001	−0.14	0.11	−0.21 to −0.07	−4.21	0.0015
	SOLma	0.20	0.14	0.11 to 0.28	4.95	0.0004	−0.03	0.07	−0.07 to 0.02	−1.32	0.2119
	SOLlp	0.09	0.11	0.02 to 0.16	2.79	0.0175	−0.04	0.05	−0.07 to −0.01	−2.95	0.0132
	SOLmp	0.20	0.09	0.14 to 0.26	7.28	< 0.0001	−0.17	0.09	−0.23 to −0.11	−6.25	< 0.0001
EDL		−0.63	0.28	−0.80 to −0.45	−7.86	< 0.0001	0.59	0.30	0.40 to 0.78	6.86	< 0.0001
TA		−0.31	0.12	−0.39 to −0.24	−9.05	< 0.0001	0.13	0.09	0.08 to 0.19	5.26	0.0003
	TAdeep	−0.28	0.18	−0.40 to −0.17	−5.58	0.0002	0.16	0.16	0.06 to 0.26	3.45	0.0053
	TAsup	−0.25	0.17	−0.36 to −014	−5.1	0.0004	0.16	0.16	0.06 to 0.27	3.34	0.0066
	TAends	−0.41	0.15	−0.50 to −0.31	−9.15	< 0.0001	0.08	0.06	0.04 to 0.12	4.43	0.0010
PER		< 0.01	0.06	−0.04 to 0.04	0.19	0.8508	0.05	0.06	0.01 to 0.09	2.64	0.0229
TP		0.01	0.05	−0.02 to 0.04	0.62	0.5451	−0.01	0.03	−0.03 to 0.01	−1.41	0.1865

Note: Amplitude estimates, SDs of the estimates, CIs, *t* values and *p* values for the strain rates (s^{-1}) along and perpendicular to the fibers for the individual lower leg muscles and muscle compartments of the TA and SOL muscle. Differences in amplitude estimates, corrected for multiple testing, are indicated in bold ($p \leq 0.0018$). $N = 12$ for all comparisons. Abbreviations: CI, confidence interval; EDL, extensor digitorum longus; GCL, gastrocnemius lateralis; GCM, gastrocnemius medialis; PER, peroneus; SD, standard deviation; SOL, soleus; SOLla, lateral anterior compartment of the soleus; SOLlp, lateral posterior compartment of the soleus; SOLma, medial anterior compartment of the soleus; SOLmp, medial posterior compartment of the soleus; TA, tibialis posterior; TAdeep, deep compartment of tibialis anterior; TAends, two compartments distal and proximal of the tibialis anterior without visible intramuscular tendon; TAsup, superficial compartment of the tibialis anterior; TP, tibialis posterior.

muscle volumes. Furthermore, strain rates were heterogeneously distributed along the length of most of the lower leg muscles and muscle compartments. The strain rate amplitudes along and perpendicular to the fibers of the EDL and GCL muscle were smaller in the loaded condition.

In agreement with our first hypothesis, the temporal strain patterns in the primary plantarflexion muscles, that is, the GCL, GCM, and SOL (and compartments), started with lengthening along and thinning perpendicular to the fibers during the dorsi-/plantarflexion movement. The primary dorsiflexion muscles of the ankle, the TA (and compartments), and EDL showed the expected opposite cyclic temporal strain rate patterns. The TP and PER muscles showed negligible average strain rate amplitudes along and perpendicular to the fibers. This is in line with their expected behavior during the dorsi-/plantarflexion movement as their primary function is to stabilize the ankle, rather than facilitate dorsi-/plantarflexion movement. The cyclic strain rate patterns observed in the plantar and dorsiflexor muscles, in combination with the absence of this pattern in the TP and PER muscles, demonstrates that the method is suitable to cover the full muscle volumes in 3D and during dynamic exercise.

Strain rate amplitudes along and perpendicular to the fibers were heterogeneously distributed over the proximodistal muscle axis in the majority of lower leg muscles, except for some of the SOL compartments and the TP muscle. The lower leg muscles with heterogeneous strain distributions primarily showed larger absolute strain rates in either the most distal or proximal segments, rather than the middle segments. A substantial number of previous studies investigated strain rate distributions in the lower leg muscles during passive lengthening and isometric contractions using 2D approaches, without correction for fiber orientations.[8,13,20,22,26,27,40,41] A few studies determined principal fiber directions by determining the fatty end layers on fast spin-echo images.[32,42] The pennation angles and fiber lengths derived using this method agreed well with ultrasound, and allow for dynamic assessments during the movement/contraction cycle, but only in single muscle and single plane. These studies confirmed that there is angular difference between the principal fiber directions and principal strain directions previously shown by Englund et al.[8] Despite this angular difference, the principal strain directions are frequently used to represent fiber compression and expansion dynamics, which are related to our strain rates along and perpendicular to the fiber. An inconsistent pattern was observed in those previous studies, where some reported homogeneous strain distributions over the muscle,[27,42,43] while others described higher strain rates in distal parts of the muscle using small region of interest-based analysis or single-slice assessments.[13,26,27,40,41,44,45] These higher strains distally are partly in line with our findings. Quite a few factors have been linked to the strain heterogeneity, for example, fiber-type distributions within the muscle, motor unit activation, and neural control, which may have had an influence on our findings.

Interestingly, in the PER muscle we did not measure a cyclic pattern on a whole muscle basis, but on a more localized level, a clear cyclic pattern with positive strain rate amplitudes along the fiber during dorsiflexion movement was observed in the most proximal segment. The PER muscle consists of three muscle heads (i.e., the peroneus longus, involved in plantarflexion and eversion of the ankle; the peroneus brevis, involved in

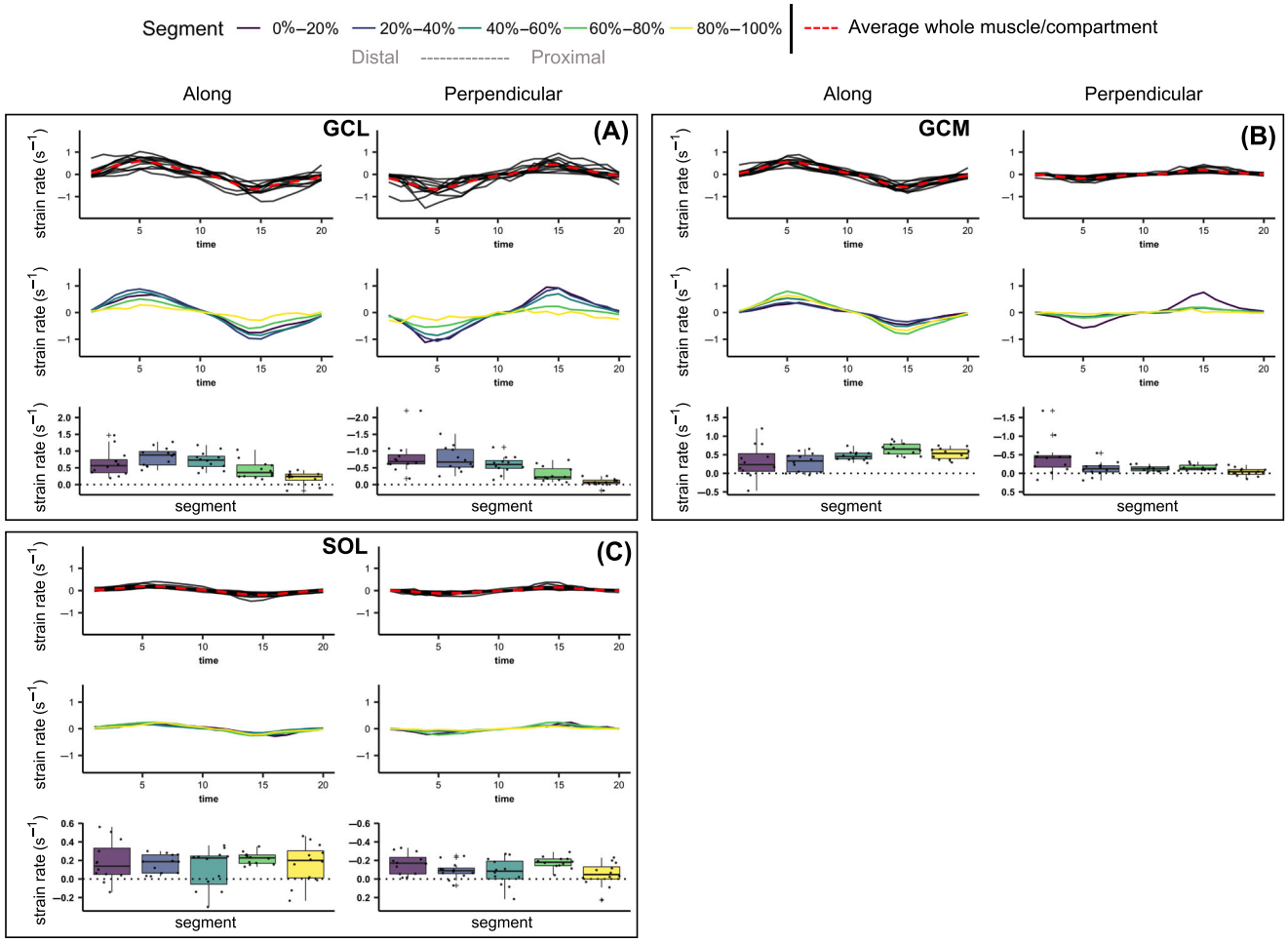

FIGURE 5 Line graphs with (top) strain rate along (left) and perpendicular (right) to the fibers in the (A) GCL, (B) GCM, and (C) SOL muscle during the full movement cycle for the exercise without load. The strain rate pattern in the full muscle volume is depicted with a red dotted line and the individual lines for each of the participants are depicted in black. The middle line graphs display strain rate along (left) and perpendicular (right) to the fibers in the (A) GCL, (B) GCM, and (C) SOL muscle during the full movement cycle for the exercise without load for the five individual segments depicted in different colors (purple 0%–20%; lilac 20%–40%; blue 40%–60%; green 60%–80%; and yellow 80%–100%). Box plots together with the individual datapoints (bottom) display strain rate amplitudes along (left) and perpendicular (right) to the fibers during maximum dorsiflexion motion without load for the individual muscle segments, with colors matching the line graphs. To facilitate comparison between the absolute amplitudes along and perpendicular to the fibers, the y-axis of the graph showing strain rate along the fibers was inverted for the muscles expected to perform a dorsiflexion movement. For the muscles expected to perform a plantarflexion movement, the y-axis of the graph of strain rate perpendicular to the fibers was inverted. Furthermore, note that the y-axis may differ between graphs and figures. GCL, gastrocnemius lateralis; GCM, gastrocnemius medialis; SOL, soleus.

plantarflexion and eversion of the ankle; and the peroneus tertius, involved in dorsiflexion and eversion of the ankle). These muscle heads are evaluated as one muscle although the origin and insertion of these heads are not equally distributed along the proximodistal muscle axis. The longus is primarily located in the most proximal muscle segments and our data suggest that there could be some selective involvement of this head during dynamic dorsi- and plantarflexion movement.

In addition to the observed heterogeneity in strain rates along the proximodistal axis, we also found variability in strain distributions in the different compartments of the SOL and TA muscles. The opposite cyclic temporal pattern in the distal segment of the TAsup compartment compared with the rest of the TA muscle, suggesting lengthening and thinning of the muscle fibers during dorsiflexion of the ankle, was rather unexpected during this dorsi-/plantarflexion movement. Currently, we do not have an explanation for this heterogeneity between compartments and segments. The fact that all muscles and compartments are interconnected via fascia and connective tissue could potentially result in intramuscular and intermuscular force transmission, which may underlie some of the displayed heterogeneity.[46,47] Furthermore, previous functional MRI studies also displayed complex activity patterns in the TA muscle, where the deep compartment showed more pronounced involvement than the superficial compartment of the TA muscle.[48] Another interesting aspect in our findings was the difference in involvement of the TA and EDL muscles during our dynamic dorsi-/plantarflexion exercise. Both muscles are primary contributors to the dorsiflexion movement, but have distinct roles

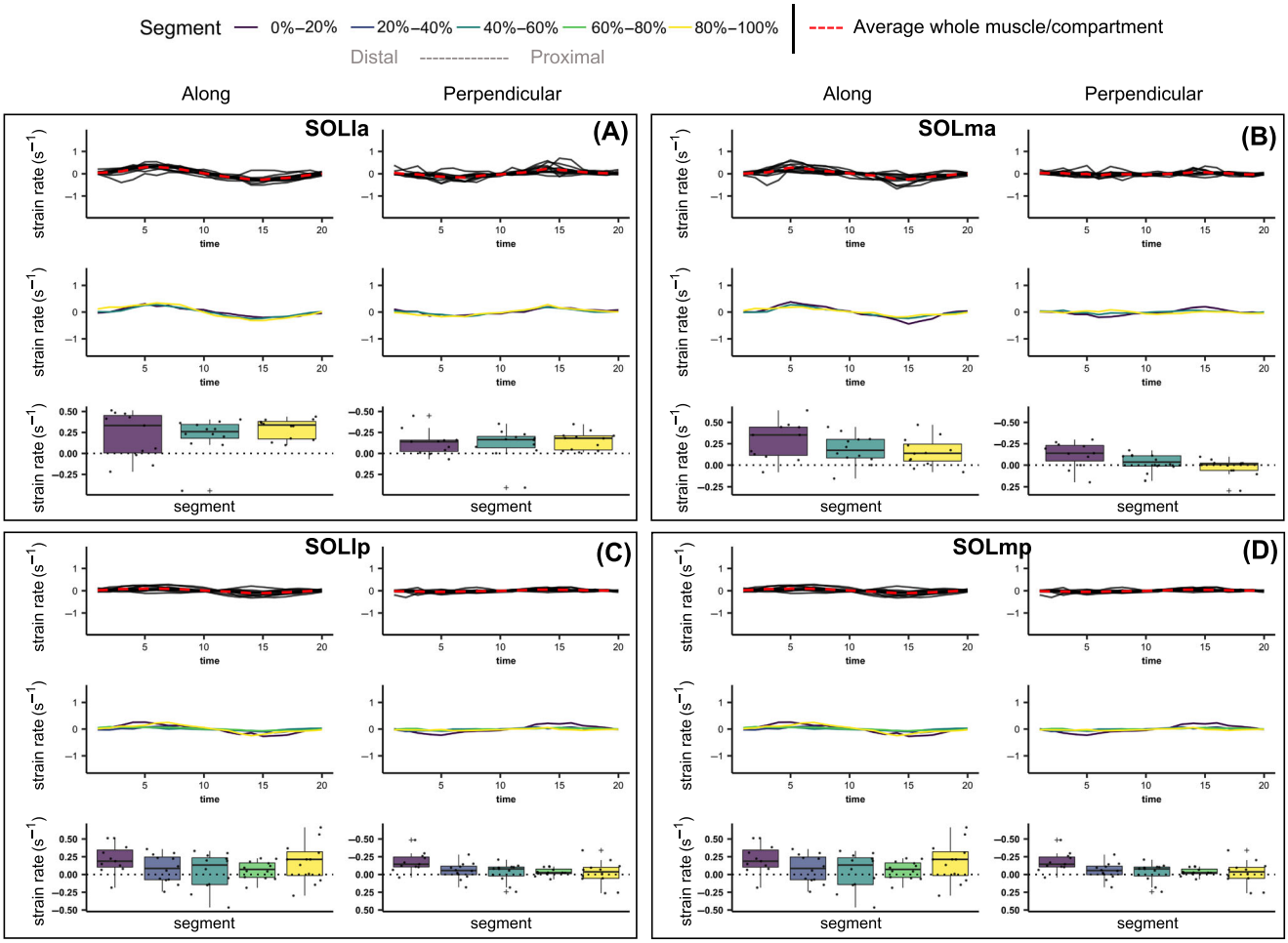

FIGURE 6 Line graphs with (top) strain rate along (left) and perpendicular (right) to the fibers in the four SOL compartments (A–D) during the full movement cycle for the exercise without load. The average strain rate pattern in the full muscle volume is depicted with a red dotted line and the individual lines for each of the participants are depicted in black. The middle line graphs display strain rate along (left) and perpendicular (right) to the fibers in the four SOL compartments (A–D) during the full movement cycle for the exercise without load for the five muscle segments depicted in different colors (purple 0%–20%; lilac 20%–40%; blue 40%–60%; green 60%–80%; and yellow 80%–100%). Box plots together with the individual datapoints (bottom) display strain rates along (left) and perpendicular (right) to the fibers during maximum dorsiflexion motion without load for the individual muscle segments, with colors matching the line graphs. Note the medial compartments of the soleus (SOLla and SOLma) are only present in the more distal part of the lower leg (see Figure 3). To facilitate the comparison between the absolute amplitudes along and perpendicular to the fibers, the y-axis of the graph with strain rate along the fibers was inverted for the muscles expected to perform a dorsiflexion movement. For the muscles expected to perform a plantarflexion movement, the y-axis of the graph showing strain rate perpendicular to the fibers was inverted. Furthermore, note that the y-axis may differ between graphs and figures. SOL, soleus; SOLla, lateral anterior compartment of the soleus; SOLlp, lateral posterior compartment of the soleus; SOLma, medial anterior compartment of the soleus; SOLmp, medial posterior compartment of the soleus.

beyond this. While the TA muscle plays an important role in ankle stabilization during walking and standing, the EDL muscle has a distinct function in toe extension.[49,50] Interestingly, our exercise setup involved a strap around the forefoot, which may have triggered a reflexive response to keep the strap in place, resulting in some additional toe extension. This factor may partially explain the observed involvement patterns.

In the majority of lower leg muscles and compartments no effect of load was observed on the strain rate amplitudes along and perpendicular to the fiber. This could be due to the relatively small load we applied in the dorsiflexion direction, as other exercise studies primarily found that larger relative loads induced changes in measured strain and strain rate patterns.[9,11,13,40,51] In the GCL and EDL muscle, lower absolute strain rate amplitudes were observed along and perpendicular to the fiber during the loaded condition compared with the unloaded condition. For the GCL muscle, this may be related to how we applied load to the ankle. In our exercise setup the load itself supported the plantarflexion movement of the ankle, which may have resulted in a lower activity level in the GCL muscle. However, to confirm any changes in muscle recruitment strategies and activation levels, PC-MRI should be validated with an independent measure.

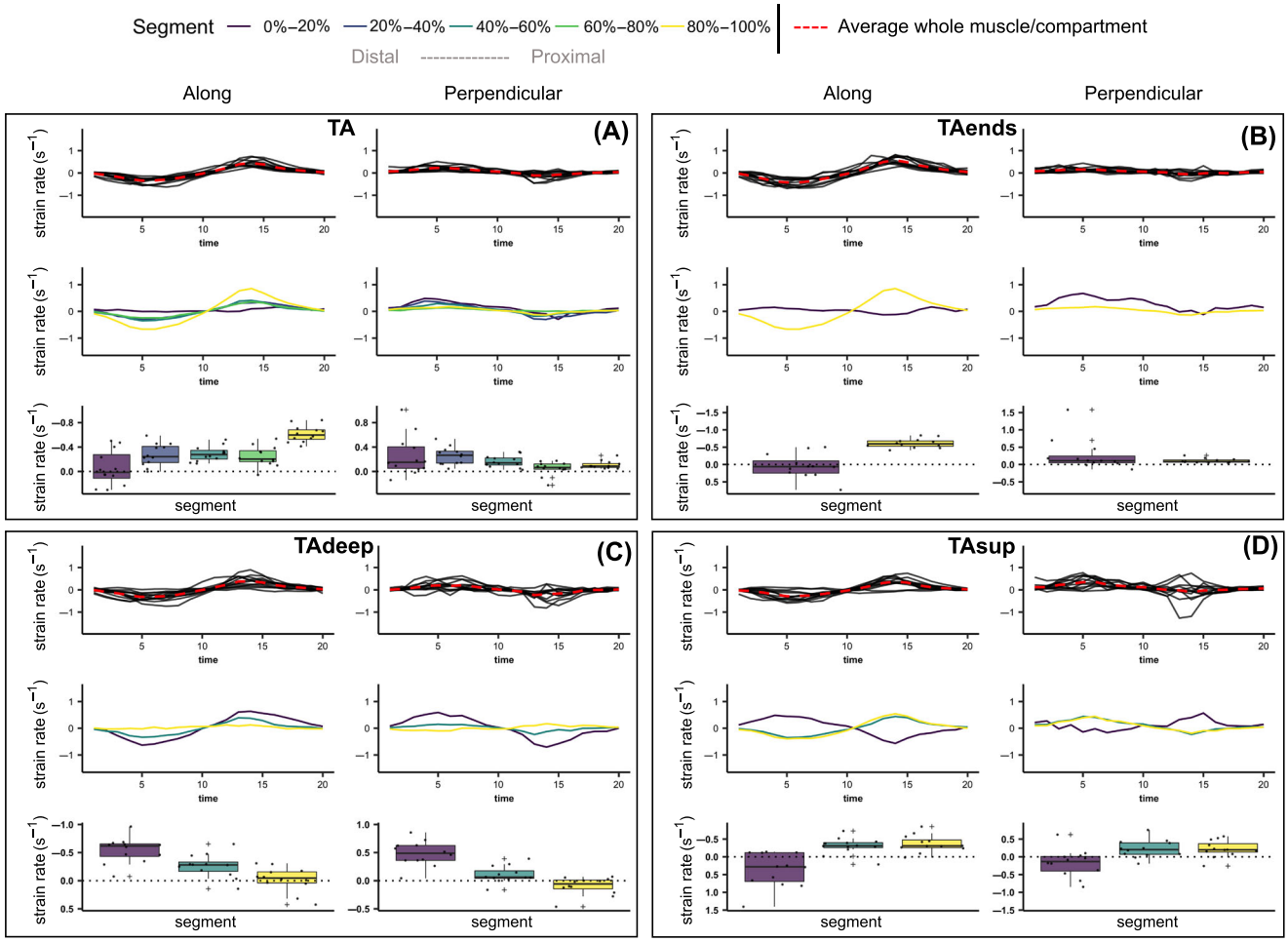

FIGURE 7 Line graphs (top) showing strain rate along (left) and perpendicular (right) to the fiber in the TA (A) and the three TA compartments (B–D) during the full movement cycle for the exercise without load. The average strain rate pattern in the full muscle volume is depicted with a red dotted line and the individual lines for each of the participants are depicted in black. The middle line graphs display strain rate along (left) and perpendicular (right) to the fiber in the TA (A) and the three TA compartments (B–D) during the full movement cycle for the exercise without load for the five individual segments depicted in different colors (purple 0%–20%; lilac 20%–40%; blue 40%–60%; green 60%–80%; and yellow 80%–100%). Box plots with the individual datapoints (bottom) display strain rates along (left) and perpendicular (right) to the fibers during maximum dorsiflexion motion without load for the individual muscle segments, with colors matching the line graphs. Note that not all compartments of TA muscle are continuously present along the proximodistal axis of the muscle (see Figure 3). To facilitate the comparison between the absolute amplitudes along and perpendicular to the fiber, the y-axis of the graph showing strain rate along the fibers was inverted for the muscles expected to perform a dorsiflexion movement. For the muscles expected to perform a plantarflexion movement, the y-axis of the graph showing strain rate perpendicular to the fibers was inverted. Furthermore, note that the y-axis may differ between graphs and figures. TA, tibialis posterior; TAdeep, deep compartment of tibialis anterior; TAends, two compartments distal and proximal of the tibialis anterior without visible intramuscular tendon; TAsup, superficial compartment of the tibialis anterior.

The approach presented in this paper will facilitate in-depth studies on muscle 3D strain heterogeneity in relation to muscle architecture, composition, and function, including properties such as fascicle lengths and curvature, (physiological) cross-sectional area, the extracellular matrix and fiber types within the muscle.[8,52,53] Furthermore, in combination with additional (imaging) techniques such as EMG, electrical stimulation,[16,54,55] and motor unit MRI,[56] more insights in motor unit activation and neural control in relation to muscle fiber strain and architecture can be obtained, which would help linking muscle contractile function to architecture and potentially to loss of function.

Our study has some limitations. First, we used the fiber orientation from the neutral (0°) ankle position to determine strain rate along and perpendicular to the fiber. During maximum dorsi- and plantarflexion and higher contraction intensities, pennation angles are known to be different compared with the neutral position.[57] This could have resulted in some underestimation or overestimation of longitudinal and transverse fiber strain rates, reducing the sensitivity of the method for actual strain rate differences. However, a deviation of 20° in the pennation angle would only cause an error of 6% strain rate (cosine [20°]), therefore it is unlikely that this explains the heterogeneity we found in strain rate amplitudes along and perpendicular to the fiber within the individual muscles, but also between individual muscles and compartments. Similarly, the participants were repositioned between the acquisition of fiber orientation and strain rates to be as comparable as possible, but this may have

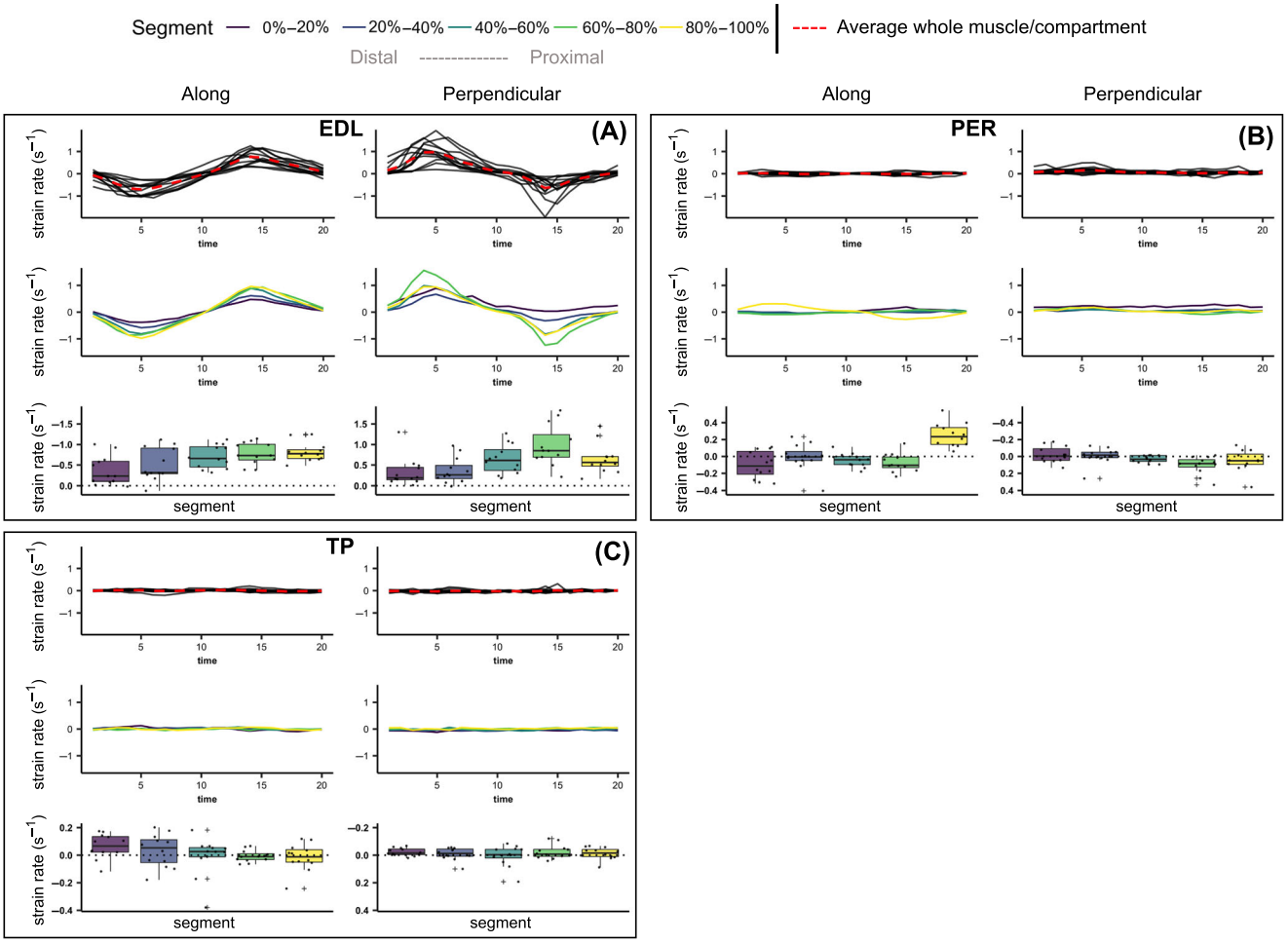

FIGURE 8 Line graphs (top) showing strain rate along (left) and perpendicular (right) to the fiber in the (A), EDL, (B) PER, and (C) TP muscle during the full movement cycle for the exercise without load. The average strain rate pattern in the full muscle volume is depicted with a red dotted line and the individual lines for each of the participants are depicted in black. The middle line graphs display strain rate along (left) and perpendicular (right) to the fiber in the (A) EDL, (B) PER, and (C) TP muscle during the full movement cycle for the exercise without load for the five individual segments depicted in different colors (purple 0%–20%; lilac 20%–40%; blue 40%–60%; green 60%–80%; and yellow 80%–100%) Box plots together with the individual datapoints (bottom) display strain rates along (left) and perpendicular (right) to the fibers during maximum dorsiflexion motion without load for the five individual muscle segments, with colors matching the line graphs. To facilitate the comparison between the absolute amplitudes along and perpendicular to the fiber, the y-axis of the graph showing strain rate along the fiber was inverted for the muscles expected to perform a dorsiflexion movement. For the muscles expected to perform a plantarflexion movement, the y-axis of the graph showing strain rate perpendicular to the fiber was inverted. Furthermore, note that the y-axis may differ between graphs and figures. EDL, extensor digitorum longus; PER, peroneus; TP, tibialis posterior.

introduced some additional noise in our outcome measures. However, it is unlikely that this explains the heterogeneity we observed in strain rate amplitudes. Third, to acquire full volume strain rate values with a time resolution of 100 ms, 216 repetitions of the movement cycle were needed. This could have led to movement variance, despite the visual tracking cue, introducing some noise in the data. We do not expect that this affected the average strain rate patterns considerably because we observed consistent patterns over all participants, but it could be the cause for the small offset observed in some of the time series, most prominent in the condition with load. Given the cyclic nature of the movement, this offset is assumed to be false. Lastly, the loaded condition was always performed after the condition without load, so there could be some fatigue effect influencing the repeatability of the movement in this condition, which might has resulted in some additional noise in our findings.

In conclusion, this study shows that DTI and PC-MRI data can be combined to measure the strain rate along and perpendicular to the fiber during dynamic exercise while covering the full lower leg. The muscles involved in the dorsi-/plantarflexion movement showed clear cyclic temporal strain rate patterns along and perpendicular to the fiber. Our data also revealed that the amplitudes of these cyclic strain rate patterns were different along the proximodistal muscle axis of most muscles and compartments. In the future, this novel approach can be a valuable tool in studies aiming to link muscle function and muscle pathology.

TABLE 2 Repeated measures ANOVA results.

			Along		Perpendicular	
Muscles	**Compartments**	**Effect**	**F value**	***p* value**	**F value**	***p* value**
GCL		Load	12.09	0.0007	18.29	< 0.0001
		Segment	29.69	< 0.0001	38.10	< 0.0001
		Load × segment	0.66	0.6227	1.54	0.1945
GCM		Load	3.48	0.0649	0.37	0.5422
		Segment	10.88	< 0.0001	10.21	< 0.0001
		Load × segment	0.47	0.7546	0.95	0.4390
SOL		Load	1.29	0.2589	0.03	0.8573
		Segment	1.14	0.3397	9.14	< 0.0001
		Load × segment	0.30	0.8741	0.58	0.6752
	SOLla	Load	0.31	0.5805	0.05	0.8223
		Segment	2.91	0.0625	1.64	0.2026
		Load × segment	0.19	0.8316	0.81	0.4506
	SOLma	Load	3.02	0.0875	0.57	0.4552
		Segment	2.82	0.0681	9.16	0.0003
		Load × segment	0.64	0.5327	0.27	0.7644
	SOLlp	Load	0.88	0.3491	0.58	0.4474
		Segment	1.33	0.2640	8.02	< 0.0001
		Load × segment	0.75	0.5601	0.32	0.8658
	SOLmp	Load	0.64	0.4239	0.38	0.5395
		Segment	4.44	0.0023	10.23	< 0.0001
		Load × segment	0.19	0.9408	0.77	0.5446
EDL		Load	12.15	0.0007	20.09	< 0.0001
		Segment	24.46	< 0.0001	19.92	< 0.0001
		Load × segment	0.65	0.6257	1.64	0.1703
TA		Load	1.00	0.3184	0.53	0.4667
		Segment	60.44	< 0.0001	8.17	< 0.0001
		Load × segment	0.37	0.8305	0.01	0.9998
	TAdeep	Load	<0.01	0.9626	0.37	0.5470
		Segment	25.80	< 0.0001	66.15	< 0.0001
		Load × segment	1.83	0.1703	0.47	0.6255
	TAsup	Load	0.23	0.6326	0.07	0.7965
		Segment	52.28	< 0.0001	16.12	< 0.0001
		Load × segment	0.08	0.9210	0.12	0.8841
	TAends	Load	0.05	0.8253	1.87	0.1814
		Segment	108.88	< 0.0001	2.25	0.1429
		Load × segment	0.73	0.3980	1.40	0.2456
PER		Load	2.48	0.1185	0.09	0.7710
		Segment	20.35	< 0.0001	10.54	< 0.0001
		Load × segment	1.95	0.1067	0.89	0.4735
TP		Load	0.15	0.6987	1.32	0.2537
		Segment	5.08	0.0009	0.89	0.4700
		Load × segment	0.14	0.9652	0.74	0.5675

Note: F values and *p* values for the main effects of condition (no load; loaded), proximodistal location (for up to five segments of 20% muscle length, see Figure 3), and the interaction effect (load*segment) for strain rate amplitudes along and perpendicular to the fibers during dorsi-/plantarflexion exercise for the individual muscles and muscle compartments are shown. Differences in strain amplitudes are indicated in bold ($p \leq 0.0018$).

Abbreviations: EDL, extensor digitorum longus; GCL, gastrocnemius lateralis; GCM, gastrocnemius medialis; PER, peroneus; SOL, soleus; SOLla, lateral anterior compartment of the soleus; SOLlp, lateral posterior compartment of the soleus; SOLma, medial anterior compartment of the soleus; SOLmp, medial posterior compartment of the soleus; TA, tibialis posterior; TAdeep, deep compartment of tibialis anterior; TAends, two compartments distal and proximal of the tibialis anterior without visible intramuscular tendon; TAsup, superficial compartment of the tibialis anterior; TP, tibialis posterior.

CONFLICT OF INTEREST STATEMENT

The authors have no conflict of interests to declare.

ORCID

Melissa T. Hooijmans https://orcid.org/0000-0002-2233-1383
Thom T. J. Veeger https://orcid.org/0000-0001-8153-8862
Valentina Mazzoli https://orcid.org/0000-0002-6700-8424
Hans C. van Assen https://orcid.org/0000-0003-4907-904X
Jurriaan H. de Groot https://orcid.org/0000-0002-7828-8863
Lukas M. Gottwald https://orcid.org/0000-0002-7394-821X
Aart J. Nederveen https://orcid.org/0000-0002-5477-973X
Gustav J. Strijkers https://orcid.org/0000-0001-6700-5058
Hermien E. Kan https://orcid.org/0000-0002-5772-7177

REFERENCES

1. Strijkers GJ, Araujo ECA, Azzabou N, et al. Exploration of new contrasts, targets, and mr imaging and spectroscopy techniques for neuromuscular disease—a workshop report of working group 3 of the biomedicine and molecular biosciences cost action BM1304 MYO-MRI. *J Neuromuscul Dis*. 2019;6(1):1-30. doi:10.3233/JND-180333
2. Bodine SC, Roy RR, Meadows DA, et al. Architectural, histochemical, and contractile characteristics of a unique biarticular muscle: the cat semitendinosus. *J Neurophysiol*. 1982;48(1):192-201. doi:10.1152/jn.1982.48.1.192
3. Gans C. Fiber architecture and muscle function. *Exerc Sport Sci Rev*. 1982;10:160-207. doi:10.1249/00003677-198201000-00006
4. Lieber RL. Skeletal muscle adaptability. I: review of basic properties. *Dev Med Child Neurol*. 1986;28(3):390-397.
5. Wokke BH, van den Bergen JC, Versluis MJ, et al. Quantitative MRI and strength measurements in the assessment of muscle quality in Duchenne muscular dystrophy. *Neuromuscul Disord*. 2014;24(5):409-416. doi:10.1016/j.nmd.2014.01.015
6. Lokken N, Hedermann G, Thomsen C, Vissing J. Contractile properties are disrupted in Becker muscular dystrophy, but not in limb girdle type 2I. *Ann Neurol*. 2016;80(3):466-471. doi:10.1002/ana.24743
7. Goodpaster BH, Park SW, Harris TB, et al. The loss of skeletal muscle strength, mass, and quality in older adults: the health, aging and body composition study. *J Gerontol A Biol Sci Med Sci*. 2006;61(10):1059-1064. doi:10.1093/gerona/61.10.1059
8. Englund EK, Elder CP, Xu Q, Ding Z, Damon BM. Combined diffusion and strain tensor MRI reveals a heterogeneous, planar pattern of strain development during isometric muscle contraction. *Am J Physiol Regul Integr Comp Physiol*. 2011;300(5):R1079-R1090. doi:10.1152/ajpregu.00474.2010
9. Sinha S, Hodgson JA, Finni T, Lai AM, Grinstead J, Edgerton VR. Muscle kinematics during isometric contraction: development of phase contrast and spin tag techniques to study healthy and atrophied muscles. *J Magn Reson Imaging*. 2004;20(6):1008-1019. doi:10.1002/jmri.20210
10. Zhong X, Epstein FH, Spottiswoode BS, Helm PA, Blemker SS. Imaging two-dimensional displacements and strains in skeletal muscle during joint motion by cine DENSE MR. *J Biomech*. 2008;41(3):532-540. doi:10.1016/j.jbiomech.2007.10.026
11. Drace JE, Pelc NJ. Skeletal muscle contraction: analysis with use of velocity distributions from phase-contrast MR imaging. *Radiology*. 1994;193(2):423-429. doi:10.1148/radiology.193.2.7972757
12. Felton SM, Gaige TA, Reese TG, Wedeen VJ, Gilbert RJ. Mechanical basis for lingual deformation during the propulsive phase of swallowing as determined by phase-contrast magnetic resonance imaging. *J Appl Physiol*. 2007;103(1):255-265. doi:10.1152/japplphysiol.01070.2006
13. Shin DD, Hodgson JA, Edgerton VR, Sinha S. In vivo intramuscular fascicle-aponeuroses dynamics of the human medial gastrocnemius during plantarflexion and dorsiflexion of the foot. *J Appl Physiol*. 2009;107(4):1276-1284. doi:10.1152/japplphysiol.91598.2008
14. Pamuk U, Karakuzu A, Ozturk C, Acar B, Yucesoy CA. Combined magnetic resonance and diffusion tensor imaging analyses provide a powerful tool for in vivo assessment of deformation along human muscle fibers. *J Mech Behav Biomed Mater*. 2016;63:207-219. doi:10.1016/j.jmbbm.2016.06.031
15. Fiorentino NM, Epstein FH, Blemker SS. Activation and aponeurosis morphology affect in vivo muscle tissue strains near the myotendinous junction. *J Biomech*. 2012;45(4):647-652. doi:10.1016/j.jbiomech.2011.12.015
16. Deligianni X, Santini F, Paoletti M, et al. Dynamic magnetic resonance imaging of muscle contraction in facioscapulohumeral muscular dystrophy. *Sci Rep*. 2022;12(1):7250. doi:10.1038/s41598-022-11147-2
17. Maurits NM, Bollen AE, Windhausen A, De Jager AE, Van Der Hoeven JH. Muscle ultrasound analysis: normal values and differentiation between myopathies and neuropathies. *Ultrasound Med Biol*. 2003;29(2):215-225. doi:10.1016/S0301-5629(02)00758-5
18. Pillen S, van Alfen N. Skeletal muscle ultrasound. *Neurol Res*. 2011;33(10):1016-1024. doi:10.1179/1743132811Y.0000000010
19. Cunningham RJ, Loram ID. Estimation of absolute states of human skeletal muscle via standard B-mode ultrasound imaging and deep convolutional neural networks. *J R Soc Interface*. 2020;17(162):20190715. doi:10.1098/rsif.2019.0715
20. Csapo R, Malis V, Sinha U, Sinha S. Mapping of spatial and temporal heterogeneity of plantar flexor muscle activity during isometric contraction: correlation of velocity-encoded MRI with EMG. *J Appl Physiol*. 2015;119(5):558-568. doi:10.1152/japplphysiol.00275.2015
21. Hooijmans MT, Niks EH, Burakiewicz J, et al. Non-uniform muscle fat replacement along the proximodistal axis in Duchenne muscular dystrophy. *Neuromuscul Disord*. 2017;27(5):458-464. doi:10.1016/j.nmd.2017.02.009

22. Malis V, Sinha U, Sinha S. Compressed sensing velocity encoded phase contrast imaging: monitoring skeletal muscle kinematics. *Magn Reson Med*. 2020;84(1):142-156. doi:10.1002/mrm.28100
23. Schlaffke L, Rehmann R, Froeling M, et al. Diffusion tensor imaging of the human calf: variation of inter- and intramuscle-specific diffusion parameters. *J Magn Reson Imaging*. 2017;46(4):1137-1148. doi:10.1002/jmri.25650
24. Boss A, Heskamp L, Breukels V, Bains LJ, van Uden MJ, Heerschap A. Oxidative capacity varies along the length of healthy human tibialis anterior. *J Physiol*. 2018;596(8):1467-1483. doi:10.1113/JP275009
25. Veeger TTJ, Hirschler L, Baligand C, et al. Microvascular response to exercise varies along the length of the tibialis anterior muscle. *NMR Biomed*. 2022;35(11):e4796. doi:10.1002/nbm.4796
26. Sinha U, Malis V, Csapo R, Moghadasi A, Kinugasa R, Sinha S. Age-related differences in strain rate tensor of the medial gastrocnemius muscle during passive plantarflexion and active isometric contraction using velocity encoded MR imaging: potential index of lateral force transmission. *Magn Reson Med*. 2015;73(5):1852-1863. doi:10.1002/mrm.25312
27. Sinha U, Malis V, Csapo R, Narici M, Sinha S. Shear strain rate from phase contrast velocity encoded MRI: application to study effects of aging in the medial gastrocnemius muscle. *J Magn Reson Imaging*. 2018;48(5):1351-1357. doi:10.1002/jmri.26030
28. Finni T, Hodgson JA, Lai AM, Edgerton VR, Sinha S. Nonuniform strain of human soleus aponeurosis-tendon complex during submaximal voluntary contractions in vivo. *J Appl Physiol*. 2003;95(2):829-837. doi:10.1152/japplphysiol.00775.2002
29. Karakuzu A, Pamuk U, Ozturk C, Acar B, Yucesoy CA. Magnetic resonance and diffusion tensor imaging analyses indicate heterogeneous strains along human medial gastrocnemius fascicles caused by submaximal plantar-flexion activity. *J Biomech*. 2017;57:69-78. doi:10.1016/j.jbiomech.2017.03.028
30. Mazzoli V, Gottwald LM, Peper ES, et al. Accelerated 4D phase contrast MRI in skeletal muscle contraction. *Magn Reson Med*. 2018;80(5):1799-1811. doi:10.1002/mrm.27158
31. Baskin RJ, Paolini PJ. Volume change and pressure development in muscle during contraction. *Am J Physiol*. 1967;213(4):1025-1030. doi:10.1152/ajplegacy.1967.213.4.1025
32. Sinha S, Shin DD, Hodgson JA, Kinugasa R, Edgerton VR. Computer-controlled, MR-compatible foot-pedal device to study dynamics of the muscle tendon complex under isometric, concentric, and eccentric contractions. *J Magn Reson Imaging*. 2012;36(2):498-504. doi:10.1002/jmri.23617
33. Lee HD, Finni T, Hodgson JA, Lai AM, Edgerton VR, Sinha S. Soleus aponeurosis strain distribution following chronic unloading in humans: an in vivo MR phase-contrast study. *J Appl Physiol*. 2006;100(6):2004-2011. doi:10.1152/japplphysiol.01085.2005
34. Gottwald LM, Peper ES, Zhang Q, et al. Pseudo-spiral sampling and compressed sensing reconstruction provides flexibility of temporal resolution in accelerated aortic 4D flow MRI: a comparison with k-t principal component analysis. *NMR Biomed*. 2020;33(4):e4255. doi:10.1002/nbm.4255
35. Klein S, Staring M, Murphy K, Viergever MA, Pluim JP. elastix: a toolbox for intensity-based medical image registration. *IEEE Trans Med Imaging*. 2010;29(1):196-205. doi:10.1109/TMI.2009.2035616
36. Froeling M, Oudeman J, van den Berg S, et al. Reproducibility of diffusion tensor imaging in human forearm muscles at 3.0 T in a clinical setting. *Magn Reson Med*. 2010;64(4):1182-1190. doi:10.1002/mrm.22477
37. Yushkevich PA, Piven J, Hazlett HC, et al. User-guided 3D active contour segmentation of anatomical structures: significantly improved efficiency and reliability. *Neuroimage*. 2006;31(3):1116-1128. doi:10.1016/j.neuroimage.2006.01.015
38. Bolsterlee B, Finni T, D'Souza A, Eguchi J, Clarke EC, Herbert RD. Three-dimensional architecture of the whole human soleus muscle *in vivo*. *PeerJ*. 2018;6:e4610. doi:10.7717/peerj.4610
39. Mauracher ME, Asmussen MJ, Nigg SR, Omu O, Jarvis SE. Portable fixed dynamometry to quantify ankle dorsiflexion force. *Muscle Nerve*. 2019;60(1):56-61. doi:10.1002/mus.26476
40. Pappas GP, Asakawa DS, Delp SL, Zajac FE, Drace JE. Nonuniform shortening in the biceps brachii during elbow flexion. *J Appl Physiol*. 2002;92(6):2381-2389. doi:10.1152/japplphysiol.00843.2001
41. Silder A, Reeder SB, Thelen DG. The influence of prior hamstring injury on lengthening muscle tissue mechanics. *J Biomech*. 2010;43(12):2254-2260. doi:10.1016/j.jbiomech.2010.02.038
42. Sinha U, Csapo R, Malis V, Xue Y, Sinha S. Age-related differences in diffusion tensor indices and fiber architecture in the medial and lateral gastrocnemius. *J Magn Reson Imaging*. 2015;41(4):941-953. doi:10.1002/jmri.24641
43. Csapo R, Malis V, Hodgson J, Sinha S. Age-related greater Achilles tendon compliance is not associated with larger plantar flexor muscle fascicle strains in senior women. *J Appl Physiol*. 2014;116(8):961-969. doi:10.1152/japplphysiol.01337.2013
44. Malis V, Sinha U, Csapo R, Narici M, Sinha S. Relationship of changes in strain rate indices estimated from velocity-encoded MR imaging to loss of muscle force following disuse atrophy. *Magn Reson Med*. 2018;79(2):912-922. doi:10.1002/mrm.26759
45. Jensen ER, Morrow DA, Felmlee JP, Murthy NS, Kaufman KR. Characterization of three dimensional volumetric strain distribution during passive tension of the human tibialis anterior using cine phase contrast MRI. *J Biomech*. 2016;49(14):3430-3436. doi:10.1016/j.jbiomech.2016.09.002
46. Oda T, Himeno R, Hay DC, et al. In vivo behavior of muscle fascicles and tendinous tissues in human tibialis anterior muscle during twitch contraction. *J Biomech*. 2007;40(14):3114-3120. doi:10.1016/j.jbiomech.2007.03.023
47. Bojsen-Moller J, Schwartz S, Kalliokoski KK, Finni T, Magnusson SP. Intermuscular force transmission between human plantarflexor muscles in vivo. *J Appl Physiol*. 2010;109(6):1608-1618. doi:10.1152/japplphysiol.01381.2009
48. Damon BM, Wadington MC, Lansdown DA, Hornberger JL. Spatial heterogeneity in the muscle functional MRI signal intensity time course: effect of exercise intensity. *Magn Reson Imaging*. 2008;26(8):1114-1121. doi:10.1016/j.mri.2008.01.023
49. Neptune RR, Kautz SA. Muscle activation and deactivation dynamics: the governing properties in fast cyclical human movement performance? *Exerc Sport Sci Rev*. 2001;29(2):76-80. doi:10.1097/00003677-200104000-00007
50. Kaminski TW, Wabbersen CV, Murphy RM. Concentric versus enhanced eccentric hamstring strength training: clinical implications. *J Athl Train*. 1998;33(3):216-221.
51. Hodgson JA, Finni T, Lai AM, Edgerton VR, Sinha S. Influence of structure on the tissue dynamics of the human soleus muscle observed in MRI studies during isometric contractions. *J Morphol*. 2006;267(5):584-601. doi:10.1002/jmor.10421
52. Adamicova K, Fetisovova Z, Malis V, Malisova S. Bloch-Sulzberg syndrome in pathology. *Cesk Patol*. 2007;43(3):109-113.
53. Blemker SS, Pinsky PM, Delp SL. A 3D model of muscle reveals the causes of nonuniform strains in the biceps brachii. *J Biomech*. 2005;38(4):657-665. doi:10.1016/j.jbiomech.2004.04.009

54. Adams GR, Harris RT, Woodard D, Dudley GA. Mapping of electrical muscle stimulation using MRI. *J Appl Physiol*. 1993;74(2):532-537. doi:10.1152/jappl.1993.74.2.532
55. Deligianni X, Pansini M, Garcia M, et al. Synchronous MRI of muscle motion induced by electrical stimulation. *Magn Reson Med*. 2017;77(2):664-672. doi:10.1002/mrm.26154
56. Heskamp L, Miller AR, Birkbeck MG, et al. In vivo 3D imaging of human motor units in upper and lower limb muscles. *Clin Neurophysiol*. 2022;141:91-100. doi:10.1016/j.clinph.2022.05.018
57. Azizi E, Brainerd EL, Roberts TJ. Variable gearing in pennate muscles. *Proc Natl Acad Sci U S A*. 2008;105(5):1745-1750. doi:10.1073/pnas.0709212105

SUPPORTING INFORMATION

Additional supporting information can be found online in the Supporting Information section at the end of this article.

How to cite this article: Hooijmans MT, Veeger TTJ, Mazzoli V, et al. Muscle fiber strain rates in the lower leg during ankle dorsi-/plantarflexion exercise. *NMR in Biomedicine*. 2024;37(3):e5064. doi:10.1002/nbm.5064